P12.190 RAINFALL OBSERVATION OF THE KU-BAND BROADBAND RADAR NETWORK IN OSAKA, JAPAN

Eiichi Yoshikawa[1,2], Satoru Yoshida[1], Takeshi Morimoto[1], Tomoo Ushio[1], Zen Kawasaki[1,3], Tomoaki Mega[4], and V. Chandrasekar[2]
Osaka University[1], Colorado State University[2],
Egypt-Japan University of Science and Technology[3], Kyoto University[4]

1. INTRODUCTION

A small-baseline weather radar network is a novel strategy to detect small-scale weather phenomena such as localized scattered thunderstorms, tornadoes, and downbursts, which often cause damage to our lives seriously. Collaborative Adaptive Sensing of the Atmosphere (CASA) [1] and X-band radar network (X-net) [2] have proposed a new radar network system using short-range X-band radars to observe lower troposphere. Compared with these, we have been proposing and developing a weather radar network consisting of Ku-band Broadband radars (BBR) [3], [4] with remarkably high range and temporal resolution.

Conventional S-, C- and X-band weather radars cover a wide area (100 through 450 km in radius) with range resolution of more than 100 m and temporal resolution of 5 min roughly, which are appropriate for precipitation systems of macro- or meso-scale. Conventional weather radars constantly observe above 1 or 2 km altitude in the most covered planer area since earth's curvature more affects in longer ranges. However, small-scale phenomena as mentioned above have a duration of 10-20 min mostly and a spatial scale of 100 m roughly, and occur in altitudes below a few kilometers [5]. Therefore, it is significantly difficult for conventional weather radars to detect these small-scale phenomena.

A weather radar network consisting of two or more BBRs can observe these small-scale phenomena with high accuracy and detection efficiency. The BBR is a short-range pulse-Doppler radar with remarkably high resolution (range and temporal resolution of several meters and 1 min per one volume scan, respectively) to detect and analyze them. The small coverage (15 km in radius) is almost never affected by earth's curvature, and the distributed radars cover a wide area. Additionally, in the radar network installation, a weather phenomenon in the overlapped areas is multi-directionally observed by several BBRs, and precipitation parameters with higher accuracy could be retrieved with a use of advanced techniques [6], [7]. These characteristics of the Ku-BBR network, the smaller coverage and higher resolution, are appropriate for urban areas densely with skyscrapers or ragged mountainous areas as in Japan.

This presentation focuses the initial observation results of the Ku-BBR network. The properties of the Ku-BBR network, spatial resolution and spatial distribution of number of observable radar nodes, minimum cross-range resolution, sensitivity, and minimum observational altitude, are elaborated in another presentation in this conference.

2. THE KU-BBR NETWORK

2.1 THE KU-BBR

The BBR transmits and receives wide-band (80 MHz (max)) signals at Ku-band (a center frequency of 15.75 GHz) to use pulse compression, which gives us high resolution and signal-to-noise ratio (SNR) for distributed scatterers (e.g., precipitation particles). High SNR achieved by pulse compression reduces to integrate coherent or incoherent pulses, and allows us to scan over the whole sky (a volume scan with 30 elevations) within a short time of 1 minute roughly. A use of a bistatic antenna system to reduce a direct coupling level (-70 dB) and not to turn a receiver off during its transmission enables the BBR to observe from a very close range of 50 m. In order to compensate strong precipitation attenuation at Ku-band, the BBR is designed as a close-range radar to a maximum range of 15 km for precipitation with a reflectivity factor above 20 dBZ with a low transmission power of

Corresponding author address: Eiichi Yoshikawa, Osaka University, Division of Electrical, Electronic and Information Engineering, Osaka, Japan, 565-0871;
email: yoshikawa@comf5.comm.eng.osaka-u.ac.jp
Colorado State University, 1373 Campus Derivery, Fort Collins, CO, 80523-1373;
email: eyoshi@engr.colostate.edu

Table I: Locational Characteristics of Radar Sites

Radar	Toyonaka	SEI	Nagisa
Latitude	34.804939°N	34.676993°N	34.840145°N
Longitude	135.455748°E	135.435054°E	135.659029°E
View	Fine	Poor (Many obstacles around notably south and north-east)	Fine
Remarks	-	Temporally installed	From Sep. 2011

10 W. These basic concepts miniaturized the BBR to be installed easily. More details of the BBR have been presented in [4]. Thus, these capabilities of the BBR are appropriate to observe small-scale phenomena.

2.2 THE KU-BBR NETWORK

Two BBRs have already been deployed in Osaka, Japan. The locational characteristics of the BBRs are shown in Table I. One is installed on the top of a building in Toyonaka campus, Osaka University, Osaka, Japan (This radar is called "Toyonaka radar", hereafter). Another is installed on a building in Osaka works of Sumitomo Electric Industries, Ltd., Osaka, Japan (This is called "SEI radar", hereafter). The baseline interval of these radars is about 14.32 km, and the area covered by both BBRs is about 294.18 km^2 in a surface of the ground, which is calculated in a maximum range of the BBR of 15 km. When observing up to 20 km with a modified observation mode (instead of the maximum range, sensitivity gets worse.), the overlapped area increases to 696.32 km^2. Now the SEI radar has many obstacles closely around, and the view of the SEI radar is limited as shown in the initial observation results. In addition, one more BBR is being installed in Nagisa sewage plant. We consider the three BBR network, which cover north Osaka area as Figure 1, is a test bed of the BBR network for both the evaluation and operation.

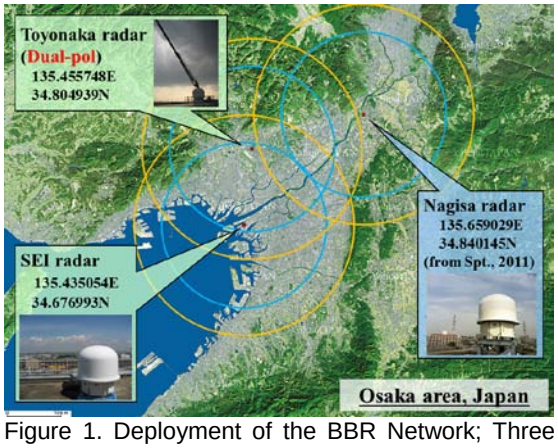

Figure 1. Deployment of the BBR Network; Three red points are on the three BBR sites, and blue and yellow circles are on 15 and 20 km ranges from each BBR site.

To output the initial results of the BBR network, precipitation attenuation is corrected by traditional Hitschfeld-Bordan (HB) solution [8] with a *k-Z* relation in Ku-band (15.75 GHz) of

$$k = 3.450 \times 10^{-4} Z_e^{\ 0.834}, \qquad (1)$$

where k and Z_e are specific attenuation in dB/km and equivalent reflectivity in mm^{6}m^{-3}, respectively [4]. It is well known that HB solution often output unacceptably large (positive) errors [9]. Therefore, retrieved reflectivities beyond 55 dBZ are neglected. In addition, retrieved reflectivities of two radars in five range bins on four adjacent beams around a desired grid point are compared, and larger values decided by a threshold are also discarded as described in Figure 2. This process also cut out saturated data by obstacles as in data of the SEI radar (see observed data in Section 3.2). Then, the

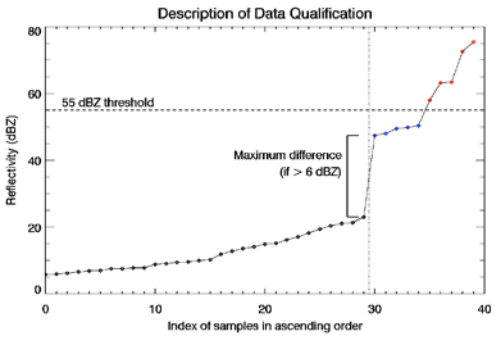

Figure 2. Description of data qualification in the BBR network; 40 samples (4 beams x 5 range bins x 2 radar nodes) around a desired Cartesian grid points are reorganized in ascending order of reflectivity. At first, samples greater than 55 dBZ (indicated by red diamond symbols) are eliminated. Then, samples indicated by blue symbols which are in the right side of the maximum difference between neighboring samples, if it is greater than 6 dBZ, are discarded.

remaining reflectivities of two radars are

Table II: Observation characteristics

	Toyonaka radar	SEI radar
Day and time	13:00 – 18:00, Sep. 14, 2010	13:00 – 18:00, Sep. 14, 2010
Operation mode	Spiral	Spiral
Azimuth rotation speed	30.0 RPM	30.0 RPM
Elevation	0 – 90 deg	0 – 90 deg
Power	10 W	10 W
Pulse length	160 μs	160 μs
Inter pulse priod	260 μs	260 μs
Pulses / segment	64	64
Waveform	Linear up-chirp	Linear up-chirp
Frequency	15.73 – 15.75 GHz	15.75 – 15.77 GHz
Weighting window	Raised-cosine window (α=0.1)	Raised-cosine window (α=0.1)

converted from each polar grid to Cartesian grid with a grid size of 20 m, and integrated by using geometric weighting functions. The weighting function for conversion from polar to Cartesian grid in each radar is expressed as

$$Z_e^{(BBR_k)} = \sum_{n=1}^{4} w_c^{(k,n)} Z_e^{(k,n)} , \qquad (2)$$

where

$$w_c^{(k,n)} = \left[\frac{\hat{\theta}_{k,n}}{\theta_h - \hat{\theta}_{k,n}} \exp\left\{ 2\sqrt{2} \ln 2 \left(\frac{1}{2}\theta_h - \hat{\theta}_{k,n} \right) \right\} + 1 \right]^{-1} ,$$

$$\left[\frac{\hat{\phi}_{k,n}}{\phi_h - \hat{\phi}_{k,n}} \exp\left\{ 2\sqrt{2} \ln 2 \left(\frac{1}{2}\theta\phi_h - \hat{\phi}_{k,n} \right) \right\} + 1 \right]^{-1}$$

$$\hat{\theta}_{k,n} = \left| \theta_{k,n} - \theta \right| ,$$

$$\hat{\phi}_{k,n} = \left| \phi_{k,n} - \phi \right| . \qquad (3)$$

θ and ϕ are azimuth and elevation angle of the desired point from each radar. θ_h and ϕ_h are -3-dB beam width. k = 1, 2 indicates each radar node in this case. The weighting function for data integration is expressed as

$$Z_e^{(INT)} = \frac{w_r^{(1)} Z_e^{(BBR_1)} + w_r^{(2)} Z_e^{(BBR_2)}}{w_r^{(1)} + w_r^{(2)}} , \qquad (4)$$

where

$$w_r^{(k)} = \left(\sum_{n=1}^{4} w_c^{(1)} g^{(k,n)}(\theta, \phi) \right)^{-1} ,$$

$$g^{(k,n)}(\theta, \phi) = \sum_{n=1}^{4} w_c^{(k,n)} \exp\left\{ -2\sqrt{2} \ln 2 \frac{\hat{\theta}_{k,n}^{\,2} + \hat{\phi}_{k,n}^{\,2}}{\theta_h^2} \right\} . \qquad (5)$$

3. INITIAL OBSERVATION

3.1 OBSERVATION CHARACTERISTICS

The two BBRs (the Toyonaka and SEI radar) were simultaneously operated in a rain event. The observational characteristics are shown in Table II. The interferences between the two BBRs are avoided by transmitting waves of different frequency bands (15.73 through 15.75 GHz for Toyonaka radar and 15.75 through 15.77 GHz for SEI radar). In this observation, both the Toyonaka and SEI radar observe whole sky (120 directions for azimuth, and 30 directions for elevation with a 3-dB beam width of 3 deg) with an update rate of 64 s not in time synchronization. The BBRs will be synchronized by a GPS in the near future.

3.2 OBSERVATION RESULTS

The initial observation results of reflectivity factor in an altitude of 1000 m in any one minute during five minute observation (from 13:54 to 13:59 on Sep. 14, 2010) are shown in Figure 3. The Toyonaka radar (Panels (a-1) through (a-5)) could not detect some north-east directions due to a closely equipped lightning rod. Since the SEI radar (Panels (b-1) through (b-5)) was interfered by many obstacles around, the received data indicate that the inputs of the ADC are saturated in many directions in the lowest elevation angle. Additionally, the SEI radar received more coupling noises also due to the obstacles.

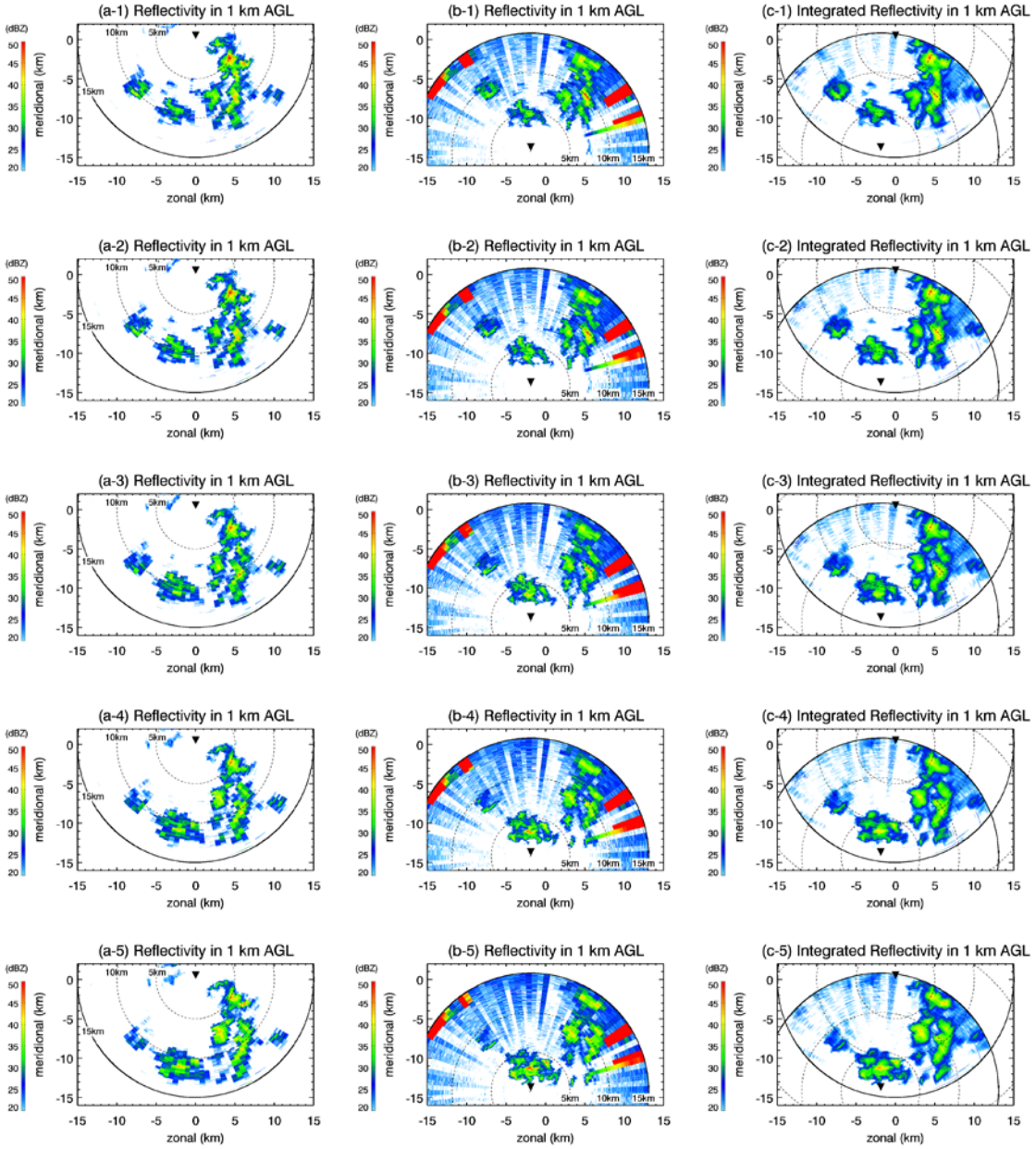

Figure 3. The initial observation results at 13:54, 55, 56, 57, and 58 on Sep. 14, 2010. Left (Panels (a-1) through (a-5)) and center (Panels (b-1) through (b-5)) panels are results of the Toyonaka and SEI radar, respectively. Right panels (Panels (c-1) through (c-5)) are integrated results from both radars. In each panel, upper and lower triangles indicate the Toyonaka and SEI radar, respectively. The two dash circles and a solid circle are on ranges of 5, 10, and 15 km from each BBR, respectively. In Panels (a-1) through (a-5) and Panels (b-1) through (b-5), circles indicate ranges from Toyonaka and SEI radar, respectively. In Panels (c-1) through (c-5), circles from both BBRs are described.

In spite of these blockages, the two BBRs detected significantly similar patterns of precipitation in the overlapped area with the high resolution, and the data integration of the BBR network provided impressive results. Panels (c-1) through (c-5) show the integrated reflectivity $Z_e^{(INT)}$ of both the radars plotted on every 20 m planar grid in the overlapped area. While being not improved around the baseline of Toyonaka and SEI radars, the precipitation patterns around 5 km in zonal range and from -10 to -2 km in meridional range, in which two composite average functions are crossed, were realistically

clarified. The blind area of the SEI radar due to overestimation of HB solution or saturations by obstacles (red colored areas in far ranges around directions for north-west and north-east) were retrieved by the Toyonaka radar. Noisy areas of the SEI radar were also restored by the Toyonaka radar with high SNR. Thus, in a BBR network, one BBR supports in an area not observed well by another BBR. Furthermore, the data integration is easily and accurately performed in the BBR network since the observational delay between the BBRs is within 1 min. For example, in the case of 4 min delay, we must integrate Panels (a-1) and (b-5) in which their shapes, positions, and magnitudes of precipitation do not agree clearly. When they are merged without any assumption and with a simple method mentioned above, the shapes are stretched wider and heavy and small rain cells are never detected. Therefore, the BBR network provides high-quality images by complimenting each other BBR, and these initial results indicate the availabilities of the BBR network to detect and analyze small-scale phenomena.

4. CONCLUSIONS

We deployed a weather radar network consisting of two BBRs, which have remarkably high range and temporal resolution of several meters and 1 min per volume scan, in the north Osaka area, Japan, and the initial observation was carried out. To output the initial results (reflectivity) of the two-BBR network, precipitation attenuation is corrected by HB solution, and multi-directional observation of both the radars compensates unacceptably large errors of HB solution and saturated data owing to obstacles around the SEI radar by comparing each other data of reflectivity. And then reflectivities of both the radar are converted from polar grid to Cartesian grid with a mesh size of 20 m, and integrated with a use of geometric weighting functions. Though the results in this paper are preliminary and validations are needed, data integration results of the two BBRs, compared with observation results of the single BBR, clearly showed fine structures of precipitation without large errors of HB solutions and saturations.

In the future, a correction for precipitation attenuation on the BBR network and an advanced integration algorithm of BBRs will be developed. Also, using the dual-polarimetric BBR (Toyonaka radar can operate dual-polarimetric observation), the dual-polarimetric measurements for precipitation at Ku-band will be assessed.

ACKNOLEDGMENT

This work was supported by a grant from Ministry of Education, Science, and Sports and Culture, Japan, and Japan Society for the Promotion of Science (JSPS).

REFERENCES

[1] F. Junyent, and V. Chandrasekar, “Theory and characterization of weather radar networks,” *J. Atmos. Ocean. Technol.*, vol. 26, pp. 474-491, 2009.

[2] M. Maki et al., “X-band polarimetric radar network in the Tokyo metropolitan area - X-NET -,” paper presented at ERAD 2008, Finnish Meteorol. Inst., Helsinki.

[3] Mega, T., K. Monden, T. Ushio, K. Okamoto, Z. Kawasaki, and T. Morimoto, “A low-power high-resolution broad-band radar using a pulse compression technique for meteorological application,” *IEEE Geosci. Remote Sens. Lett.*, 4(3), 392–396, 2007.

[4] Yoshikawa, E., T. Ushio, Z. Kawasaki, T. Mega, S. Yoshida, T. Morimoto, K. Imai, and S. Nagayama, “Development and initial observation of high-resolution volume-scanning radar for meteorological application,” *IEEE Trans. Geosci. Remote Sens.*, 48, 3225–3235, 2010.

[5] R. A. Houze, Jr., Cloud Dynamics, San Diego, CA: Academic, 1993.

[6] V. Chandrasekar and S. Lim, “Retrieval reflectivity in a networked radar environment,” *J. Atmos. Ocean. Technol.*, vol. 25, pp. 1755-1767, 2008.

[7] G. Zhang, Tian-You Yu, and R. J. Doviak, “Angular and range interferometry to refine weather radar resolution,” *Radio Sciense*, vol. 40, 2005.

[8] W. Hitschfeld, and J. Bordan, “Errors inherent in the radar measurement of rainfall at attenuating wavelengths,” *J. of Meteorol.*, vol. 11, pp. 58-67, 1954.

[9] T. Iguchi, and R. Meneghini, “Intercomparison of single-frequency methods for retrieving a vertical rain profile from airborne or spaceborne radar data,” *J. Atmos. Ocean. Technol.*, vol. 11, pp. 1507-1516, 1994.